2011

Fast localized wavefront correction using area-mapped phase-shift interferometry

G. Hall

Gabriel C. Spalding
Haverford College

P. J. Campagnola

J. G. White

K. W. Eliceiri

Fast localized wavefront correction using area-mapped phase-shift interferometry

Gunnsteinn Hall,[1] Gabriel C. Spalding,[2] Paul J. Campagnola,[1] John G. White,[1] and Kevin W. Eliceiri[1,*]

[1]*Department of Biomedical Engineering & Laboratory for Optical and Computational Instrumentation, University of Wisconsin—Madison, 1675 Observatory Drive, Madison, Wisconsin 53706, USA*

[2]*Department of Physics, Illinois Wesleyan University, Illinois 61701, USA*

**Corresponding author: eliceiri@wisc.edu*

Received May 16, 2011; accepted June 22, 2011;
posted July 1, 2011 (Doc. ID 147642); published July 27, 2011

We propose an innovative method for localized wavefront correction based on area-mapped phase-shift (AMPS) interferometry. In this Letter, we present the theory and then experimentally compare it with a previously demonstrated method based on spot-optimized phase-stepping (SOPS) interferometry. We found that AMPS outperforms SOPS interferometry in terms of speed by threefold, although in noisy environments the improvements may be larger. AMPS yielded similar point-spread functions (PSF) as SOPS for moderate system-induced aberrations, but yielded a slightly less ideal PSF for larger aberrations. The method described in this Letter may prove crucial for applications where the phase-stepping solution does not have sufficient speed. © 2011 Optical Society of America

OCIS codes: 110.1080, 110.0113, 110.2650, 090.1000, 230.6120, 070.6120.

Optical systems often exhibit aberrations that decrease the amplitude and resolution below that predicted by the idealized point-spread function (PSF). Typically, the first step towards correction involves obtaining a map of the aberrated wavefront. For some applications this is readily accessible and can be sampled using a wavefront sensor (WFS). In many optical systems this is not possible. For example, in multiphoton laser-scanning microscopy (MPLSM) the intensity of the fluorescence signal critically depends on the focal volume [1]. As light travels through an optically inhomogeneous tissue, different rays are delayed by varying amounts, especially when high-numerical aperture objectives are used. To remedy this, nondeterministic algorithms have been used to search the phase-correction space to optimize a certain metric such as fluorescence intensity [2–4]. However, those may fail for high-spatial frequency phase changes since usually only the lower frequencies are probed, due to time and mirror deformability constraints. Other approaches have sampled the wavefront of back-scattered light from the focal region using a WFS [5,6]. The disadvantage is that the back-scattered beam travels out of the tissue and does not fully represent the state at the focal point.

Recently, deterministic methods have been developed for aberration correction. Vellekoop *et al.* achieved optimal light transport through tissue by changing the phase of each pixel of a spatial light modulator (SLM) to optimize a single pixel on a CCD camera [7]. Čižmár *et al.* and Ji *et al.* applied related techniques for optical trapping [8] and MPLSM [9], respectively. Finally, Bowman *et al.* demonstrated a sensitive method, utilizing an SLM as a Shack–Hartmann WFS to display a grid of focal points to measure and correct the aberrations [10].

In this Letter we analyze the technique proposed by Čižmár *et al.* and Ji *et al.* in terms of Fourier optics and demonstrate an innovative and faster method based on the same instrumentation. We emphasize that both methods optimize the focus at a single location. This is important because, when focusing through aberrated media, such as turbid biological samples, different spots may require different corrections [8].

Figure 1 shows the experimental setup (a) and illustrates the division of the SLM into N^2 regions (b). Two regions are made active at a time, the scan region (indexed j) and the reference region (indexed k). Figure 1(c) illustrates the basis of the two techniques. The regions are "activated" by applying a phase gradient to those regions only. The light source is a mode-locked ultrafast Coherent Mira 900 laser, outputting a beam of wavelength 780 nm, which is then filtered and expanded to overfill the SLM.

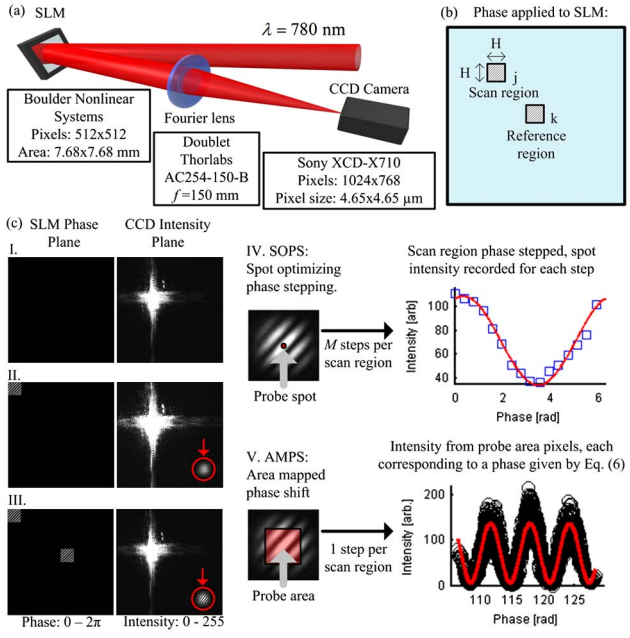

Fig. 1. (Color online) (a) Experimental setup. (b) Definition of scan and reference regions. (c) Illustration of the SOPS and AMPS methods. I: Flat SLM and corresponding zero-order diffraction. II: Scan region activated by applying a phase gradient. Corresponding scan region's PSF appears on the CCD (circled). III: Reference region activated and an interferogram appears (circled) (Media 1). IV: SOPS (Media 2), V: AMPS (Media 3).

A theoretical framework is now presented to analyze the method of [8,9] in terms of Fourier optics, upon which we will base our novel method. The object plane (SLM) optical field [see Fig. 1(b)] can be written

$$O_{jk}(x,y) = e^{i2\pi(xT_x+yT_y)}\left[e^{i\phi_j}\mathrm{rect}\left(\frac{x-x_j}{H}\right)\mathrm{rect}\left(\frac{y-y_j}{H}\right) + e^{i\phi_k}\mathrm{rect}\left(\frac{x-x_k}{H}\right)\mathrm{rect}\left(\frac{y-y_k}{H}\right)\right]. \quad (1)$$

Applying the Fourier transform, the irradiance in the image plane (on the CCD) is

$$I(x_i,y_i) = |W(x_i,y_i)|^2 \cdot \left[2+2\cos\left(-\frac{2\pi}{f\lambda}(D_x x_i + D_y y_i) + \Delta\phi\right)\right]. \quad (2)$$

Here we have defined (for simplification)

$$W(x_i,y_i) = H^2\mathrm{sinc}\left[\left(\frac{x_i}{\lambda f} - T_x\right)H\right]\cdot\mathrm{sinc}\left[\left(\frac{y_i}{\lambda f} - T_y\right)H\right], \quad (3)$$

where H is the region height andD_x and D_y are the respective horizontal and vertical distances between the scan and reference regions. The function $W(x_i,y_i)$ represents the window where the interferogram is visible and the phase gradient parameters T_x and T_y control its location.

The method that we refer to as spot-optimized phase-stepping (SOPS) wavefront correction method adds a phase ϕ_s to the scan region only. This phase is stepped from 0 to 2π in M steps and the intensity at spot location (x_{i0},y_{i0}) is recorded. Intensity as a function of scan phase can then be written as

$$R_{\mathrm{SOPS}}(\phi_s) = |W(x_{i0},y_{i0})|^2 \cdot \left[2+2\cos\left(-\frac{2\pi}{f\lambda}(D_x x_{i0} + D_y y_{i0}) + \Delta\phi + \phi_s\right)\right]. \quad (4)$$

By fitting to the cosine term, the phase offset can be determined:

$$(\phi_s)^{\mathrm{fit}} = \phi_{\mathrm{opt}} = \frac{2\pi}{f\lambda}(D_x x_{i0} + D_y y_{i0}) - \Delta\phi. \quad (5)$$

The fit equals the optimal phase ϕ_{opt} which makes the scan and reference region arrive in phase and is the condition for optimal focusing. By iteratively moving the scan region and finding the phase offset for each region, a phase map for the whole SLM can be found. One disadvantage of the SOPS protocol is that it requires a minimum number, M, of three phase-steps per region to fully sample the cosine function. However, a higher number of steps (and thus data points) increases the accuracy of the phase map and is thus slower.

Instead of stepping the phase of the scan region, we suggest using the spatially varying phase in the image plane, which creates the interferogram [Fig. 1(c) V), to obtain the correction. This method will be referred to as the area-mapped phase-shift (AMPS) method.

To exploit this information, we combine the spatially varying phase terms of the cosine in Eq. (2) into a single phase term as follows:

$$\phi_a = -\frac{2\pi}{f\lambda}(D_x x_i + D_y y_i). \quad (6)$$

Each pixel within the probe area has an associated value of ϕ_a and an intensity value. The intensity as a function of the spatially varying phase (ϕ_a) can be written as

$$R_{\mathrm{AMPS}}(\phi_a) = |W(x_i,y_i)|^2[2+2\cos(\Delta\phi+\phi_a)]. \quad (7)$$

By fitting $R_{\mathrm{AMPS}}(\phi_a)$ to a cosine we find $(\phi_a)^{\mathrm{fit}} = -\Delta\phi$, and, by comparison with Eq. (5), we have

$$\phi_{\mathrm{opt}} = \frac{2\pi}{f\lambda}(D_x x_{i0} + D_y y_{i0}) + (\phi_a)^{\mathrm{fit}}. \quad (8)$$

Since all terms in this equation are known, the phase offset can then be calculated. A correction map for the whole SLM is obtained by repeating this for all regions.

The run time for both methods is given by

$$T = MN^2(T_{\mathrm{CCD}} + T_{\mathrm{SLM}} + T_{\mathrm{delays}}) = MN^2 T_{\mathrm{iteration}}. \quad (9)$$

In our setup, the time per iteration is approximately 55 ms (18 Hz), corresponding to 0.88 s, 3.52 s, and 49.5 s for 4×4, 8×8, and 30×30 region corrections, respectively, for AMPS ($M=1$). The corresponding SOPS corrections require at least three times longer to achieve optimization.

For validation, AMPS was compared with the SOPS method. Figure 2 shows results of correcting system aberrations with increasing number of regions (increasing wavefront detail). Figure 2(a) shows the retrieved wavefronts from both methods. Figure 2(b) shows the resulting PSFs of our new approach. Figure 2(c) plots the increase in PSF peak intensity with increasing wavefront detail. For AMPS and SOPS, the peak intensity increases were 83% and 82%, respectively. In addition, the mean intensity of pixels within the full-width half-maximum (FWHM) is shown and follows the same behavior as the peak intensity. Lastly, in Fig. 2(d), the radial profiles of the PSFs are shown and compared with that of the theoretical system. Both methods give nearly diffraction-limited performance.

In order to evaluate AMPS for correcting larger aberrations, an aberrated glass [Fig. 3(a)] was inserted in front of the focusing lens. Both correction methods were applied using 900 (30×30) regions and Fig. 3(b) shows the retrieved wavefronts. Figure 3(c) shows the PSFs corresponding to no correction (N/C) (I), AMPS correction (II) and SOPS correction (III). In addition, the radial profiles are shown and compared with the idealized system profile in Fig. 3(d). Without correction, the PSF is highly diffuse and has weak intensity. Both AMPS and SOPS provide significant improvements and are comparable with the idealized system profile. It is worth noting that SOPS gave a 23.74% higher peak intensity than AMPS in this case. In terms of PSF width (or resolution), our setup was unable to resolve a difference within experimental error, due to the limiting pixel size.

Each correction is localized to a chosen focal location, which is controlled through the phase gradients T_x and

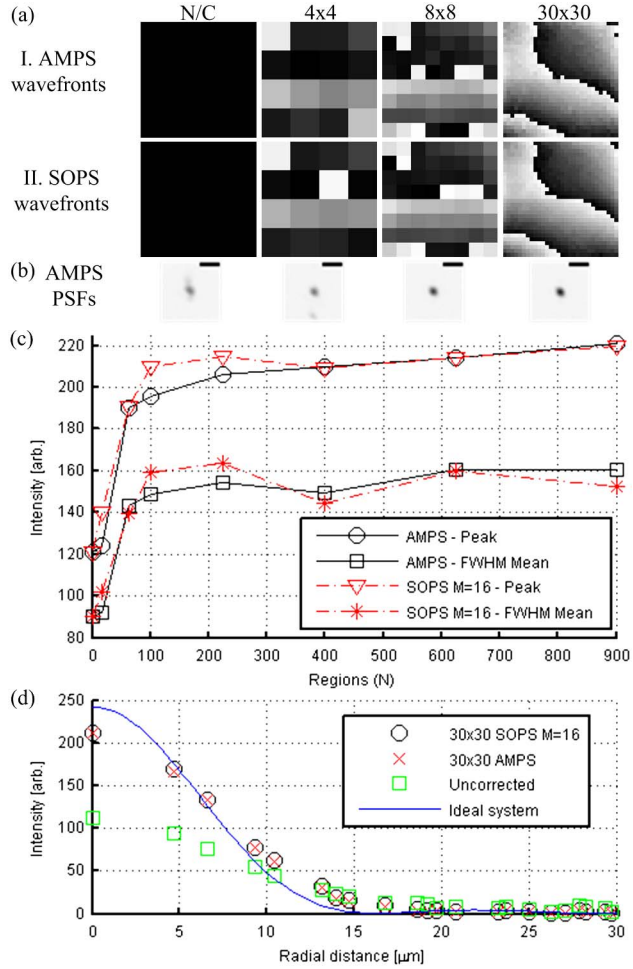

Fig. 2. (Color online) System wavefront corrections. (a) Wavefronts obtained with AMPS (I) and SOPS (II). The number of regions used is indicated. (b) PSFs corresponding to the AMPS wavefront. Size of the scale bar is 50 μm. (c) Effect of wavefront detail on PSF intensity (both peak and FWHM averaged). (d) Radial PSF comparisons for AMPS, SOPS, uncorrected and ideal systems. (N/C: no correction).

T_y. When applying a correction and moving the focus away from its nominal location we noted a drop-off in PSF intensity, increasingly with larger displacements. This was more noticeable for larger aberrations, as expected.

The AMPS method is very dependent on the validity of our theory, as the correction phase of Eq. (8) includes calculated components. In contrast, the SOPS method is less sensitive as the phase comes directly from fitting. However, this comes at the cost of speed as SOPS is theoretically three times slower and, in practice, may be yet slower for obtaining good fits. For example we used $M = 16$ for our comparisons (sixteenfold slower). We also note that using $M = 3$ resulted in similar PSF improvements. When applying the method in a biological specimen, it is reasonable to expect more noise sources, in which case more data points may be required for fitting.

In summary, we have presented a localized wavefront correction method (AMPS) that performs at least three times faster than the previously published method [8,9], with similar degree of correction for moderate aberration and only slightly reduced fidelity for larger aberrations. The method is easy to add to a system already implementing SOPS. Then, weighing the importance of accuracy and speed, could reasonably guide the choice of methods for a given experiment.

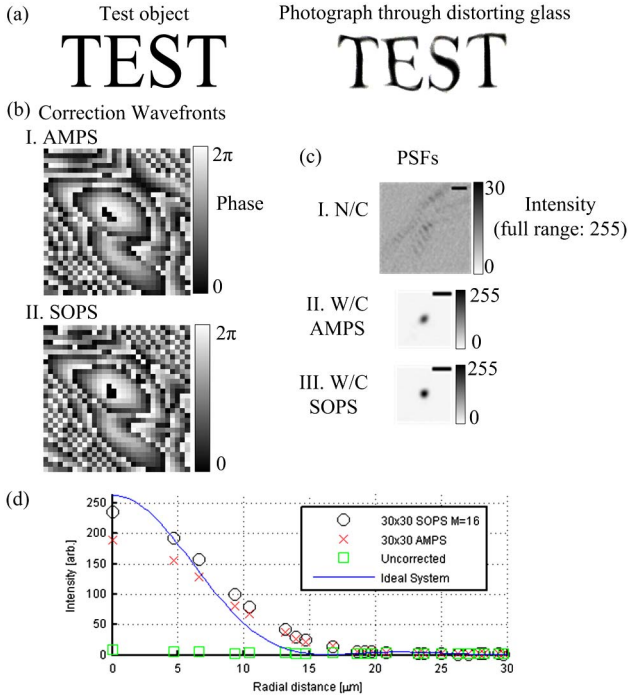

Fig. 3. (Color online) Highly aberrated glass. (a) Illustration of the nature of the aberration through a photograph. (b) AMPS and SOPS retrieved wavefronts. (c) PSFs without (N/C) and including corrections. Scale bar size is 50 μm. (d) Comparison of PSF radial profiles with the ideal system profile.

We gratefully acknowledge support from National Institute of Health (NIH) National Institute of Biomedical Imaging and Bioengineering (NIBIB) R01-EB000184, National Science Foundation (NSF) Chemical, Bioengineering, Environmental, and Transport Systems (CBET) 0959525 and the Wisconsin Institutes for Discovery. G. H. acknowledges support from a Leifur Eiríksson Foundation Scholarship. G. C. S. acknowledges the donors of the American Chemical Society Petroleum Research Fund for partial support of this research.

References

1. W. Denk, J. H. Strickler, and W. W. Webb, Science **248**, 73 (1990).
2. P. N. Marsh, D. Burns, and J. Girkin, Opt. Express **11**, 1123 (2003).
3. M. Booth, M. A. A. Neil, and T. Wilson, J. Microsc. **192**, 90 (1998).
4. S. P. Poland, A. J. Wright, and J. M. Girkin, Appl. Opt. **47**, 731 (2008).
5. M. Rueckel, J. A. Mack-Bucher, and W. Denk, Proc. Natl. Acad. Sci. USA **103**, 17137 (2006).
6. J. W. Cha, J. Ballesta, and P. T. C. So, J. Biomed. Opt. **15**, 046022 (2010).
7. I. M. Vellekoop and A. P. Mosk, Opt. Commun. **281**, 3071 (2008).
8. T. Čižmár, M. Mazilu, and K. Dholakia, Nat. Photonics **4**, 388 (2010).
9. N. Ji, D. E. Milkie, and E. Betzig, Nat. Methods **7**, 141 (2009).
10. R. W. Bowman, A. J. Wright, and M. J. Padgett, J. Opt. **12**, 124004 (2010).